Climate
of the Past

Discussions

Open Access

EGU

Antarctic temperature and CO_2: near-synchrony yet variable phasing during the last deglaciation

Jai Chowdhry Beeman[a,1], Léa Gest[a,1], Frédéric Parrenin[a], Dominique Raynaud[a], Tyler J. Fudge[b], Christo Buizert[c], and Edward J. Brook[c]

[a]Univ. Grenoble Alpes, CNRS, IRD, IGE, F-38000 Grenoble, France
[b]Department of Earth and Space Sciences, University of Washington, Seattle, WA 98195, USA
[c]College of Earth, Ocean, and Atmospheric Sciences, Oregon State University, Corvallis, OR 97331, USA
[1]Jai Chowdhry Beeman and Léa Gest contributed equally to this work.

Correspondence to: Frédéric Parrenin frederic.parrenin@univ-grenoble-alpes.fr

Abstract. The last deglaciation, which occurred from 18,000 to 11,000 years ago, is the most recent large natural climatic variation of global extent. With accurately dated paleoclimate records, we can investigate the timings of related variables in the climate system during this major transition. Here, we use an accurate relative chronology to compare regional temperature proxy data and global atmospheric CO_2 as recorded in Antarctic ice cores. We build a stack of temperature variations by averaging the records from five ice cores distributed across Antarctica, and develop a volcanic synchronization to compare it with the high-resolution, robustly dated WAIS Divide CO_2 record. We assess the CO_2 / Antarctic temperature phase relationship using a stochastic method to accurately identify the probable timings of abrupt changes in their trends. During the large, millenial-scale changes at the onset of the last deglaciation at 18 ka and the onset of the Holocene at 11.5 ka, Antarctic temperature most likely led CO_2 by several centuries. A marked event in both series around 16 ka began with a rapid rise in CO_2, which stabilized synchronously with temperature. CO_2 and Antarctic temperature peaked nearly synchronously at 14.4 ka, the onset of the Antarctic Cold Reversal (ACR) period. And CO_2 likely led Antarctic temperature by around 250 years at the end of the ACR. The five major changes identified for both series are coherent, and synchrony is within the 2σ uncertainty range for all of the changes except the Holocene onset. But the often-multimodal timings, centennial-scale substructures, and likely-variable phasings we identify testify to the complex nature of the two series, and of the mechanisms driving the carbon cycle and Antarctic temperature during the deglaciation.

1 Introduction

Glacial-interglacial transitions, or deglaciations, mark the paleorecord approximately every 100,000 years over the past million years or so (Jouzel et al., 2007; Lisiecki and Raymo, 2005; Williams et al., 1997). The last deglaciation, often referred as glacial termination 1 (T1), offers a case study for a large global climatic change, very likely in the 3-8°C range on the global scale (Masson-Delmotte et al., 2013), and thought to be initiated by an orbitally driven insolation forcing (Berger, 1978; Hays et al., 1976; Kawamura et al., 2007). The canonical interpretation of this apparent puzzle is that insolation acts as a pacemaker of climatic cycles and the amplitude of glacial-interglacial transitions is mainly driven by two strong climatic feedbacks:

atmospheric CO_2 and continental ice surface-albedo changes. However, the exact role of atmospheric CO_2, as well as the mechanisms that control the CO_2 rise, are still a matter of debate. Accordingly, reconstructing the phase relationship (leads and lags) between climate variables and CO_2 during the last termination has become of importance, and has a substantial history in ice core research (Barnola et al., 1991; Caillon et al., 2003; Parrenin et al., 2013; Pedro et al., 2012; Raynaud and Siegenthaler,

5   1993).

Global temperature has been shown to consistently lag CO_2 (Shakun et al., 2012) during T1, supporting the importance of CO_2 as an amplifier of orbitally-driven global-scale warming. But Antarctic temperature and CO_2 concentrations changed much more coherently as T1 progressed, and did not increase continuously. Indeed, near the end of the glacial-interglacial transition, Antarctic warming slowed and even reversed during a period of about 2000 years, coinciding with a warm period in

10   the North called the Bølling–Allerød (B/A). This period of cooling in Antarctica is called the Antarctic Cold Reversal (ACR). A period of cooling in the Northern Hemisphere known as the Younger Dryas (YD), followed the B/A, coinciding with a period of warming in the SH.

High-latitude Southern Hemisphere paleotemperature series–including Southern Ocean temperature–varied similarly to Antarctic temperature during T1 (Shakun et al., 2012; Pedro et al., 2016). In addition, the Southern Ocean is thought to haved

15   played an important role in the CO_2 increases. A weakening of the oceanic biological carbon pump, combined with Southern Ocean upwelling, is thought to have dominated the deglacial CO_2 increase until 15.5 ka, when rising ocean temperature likely began to play a role as well (Bauska et al., 2016). The phase relationship with Antarctic temperature can provide additional information to characterize the mechanisms of the T1 CO_2 rise.

Ice sheets are exceptional archives of past climates and atmosphere composition. Local temperature is recorded in the

20   isotopic composition of snow/ice (Jouzel et al., 2007; NorthGRIP Project Members, 2004) thanks to the so-called isotopic paleothermometer (Lorius and Merlivat, 1975; Johnsen et al., 1989). The concentration of continental dust in ice sheets is a proxy of continental aridity, atmospheric transport intensity and precipitation (Petit and Delmonte, 2009; Lambert et al., 2012). Finally, air bubbles enclosed in ice sheets are near-direct samples of the past atmosphere. However, the age of the air bubbles is younger than the age of the surrounding ice, since air is locked in at the base of the firn (approximately 100 m below the surface

25   on the East Antarctic plateau) at the Lock-In Depth (LID) (Parrenin et al., 2012). The firn, from top to bottom, is composed of a convective zone (CZ) where the air is mixed vigorously, and a diffusive zone (DZ) where molecular diffusion dominates transport. Firn densification models can be used to estimate the LID and the corresponding age difference (Sowers et al., 1992).

Atmospheric CO_2 concentrations, recorded in the air bubbles enclosed in ice sheets, are better preserved in Antarctic ice than in Greenland ice, because the latter has much higher concentrations of organic material and carbonate dust (Raynaud

30   et al., 1993). Measured essentially on the Vostok and EPICA Dome C ice cores, the long ice core record of CO_2 (Lüthi et al., 2008) covers the last 800 ka. This record is of global significance.

Early studies suggested that at the initiation of the termination around 18 ka B1950 (kiloyears before 1950 A.D.), just after the Last Glacial Maximum (LGM), Antarctic temperature started to warm 800 ± 600 yr before CO_2 began to increase (Monnin et al., 2001), a result that was sometimes misinterpreted to mean that CO_2 was not an important amplification factor of the

35   deglacial temperature increase. This study used measurements from the EPICA Dome C (EDC) ice core (Jouzel et al., 2007)
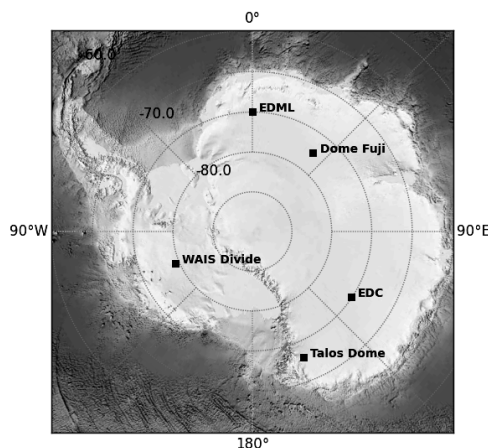
Climate
of the Past

Open Access

EGU

Discussions

Figure 1. Drilling locations of the ice cores from which the CO_2 and isotopic paleotemperature records included in this study were measured.

and used a firn densification model to determine the air chronology. However, this firn densification model was later shown to be in error by several centuries for low accumulation sites such as EDC during glacial periods (Loulergue et al., 2007; Parrenin et al., 2012).

Two more recent works (Pedro et al., 2012; Parrenin et al., 2013), used stacked temperature records and improved estimates
5   of the age difference between ice and air records to more accurately estimate the relative timing of changes in Antarctic temperature and atmospheric CO_2 concentration. In the first of these studies, measurements from the higher accumulation ice cores at Siple Dome and Law Dome, used to decrease the uncertainty in the ice-air age shift, indicated that CO_2 lagged Antarctic temperature by 0-400 yr on average during the last deglaciation (Pedro et al., 2012). The second study (Parrenin et al., 2013) used measurements from the low accumulation EDC ice core but circumvented the use of firn densification models by
10 using the nitrogen isotope ratio $\delta^{15}N$ of N_2 as a proxy of the DZ height, hypothesizing that the height of the CZ was negligible during the study period. CO_2 and Antarctic temperature were found to be roughly in phase at the beginning of TI and at the end of the ACR period, but CO_2 was found to lag Antarctic temperature by several centuries at the beginning of the Antarctic Cold Reversal and Holocene periods.

A new CO_2 record of unprecedented high resolution (Marcott et al., 2014) from the West Antarctic Ice Sheet (WAIS)
15 divide ice core merits the reopening of this investigation. The air chronology of WAIS Divide is well constrained thanks to a relatively high accumulation rate and to accurate nitrogen-15 measurements (Buizert et al., 2015). The WAIS record evidences centennial-scale changes in the global carbon cycle during the last deglaciation superimposed on more gradual, millenial-scale trends that bear resemblance to Antarctic temperature (Marcott et al., 2014).

The deglacial temperature rise seen at WAIS Divide (WD) is structurally similar to that at other Antarctic sites. However,
20 West Antarctic warming may have been greater in magnitude than East Antarctic warming by up to 3 degrees, and the rise

in West Antarctic temperature shows early warming starting around 21 ka B1950, following local insolation (Cuffey et al., 2016). This early warming trend is much more gradual in records from East Antarctic ice cores. The difference between the two records may be related to sea ice conditions around East and West Antarctica, and perhaps to elevation changes (Cuffey et al., 2016; WAIS Divide Project Members and others, 2013). However, the temperature record at WAIS Divide shows an

5 acceleration in warming around 18 ka B1950 which is also present in East Antarctic records (WAIS Divide Project Members and others, 2013).

In the present work we refine our knowledge of leads and lags between Antarctic temperature and CO_2. We develop a new stack of accurately synchronized Antarctic temperature records to reduce local signals, placed using volcanic matching on the WAIS Divide chronology (WD2014). We then compare the temperature stack to the high resolution WAIS Divide CO_2 record

10 by determining the probable timings of changes in trend.

2 Methods and data

2.1 Temperature stack and ice chronology

We develop a stack of isotopic temperature records (Antarctic Temperature Stack 2, or ATS2) in order to remove local influences and noise in the individual records to the greatest extent possible. Our stack contains five records: EDC, Dome Fuji (DF),

15 Talos Dome (TALDICE), EPICA Dronning Maud Land (EDML) and WAIS Divide (WD). We use previously published ties between EDC, DF, TALDICE and EDML (Parrenin et al., 2013; Fujita et al., 2015). We then develop a volcanic synchronization between the EDC and WD cores (Figure 2) to place our stack on the WD2014 chronology (Buizert et al., 2015; Sigl et al., 2015). The Vostok record, included in the stack used by Parrenin et al. (2013) is excluded: it contains additional chronological uncertainty as it is derived using records from two drilling sites.

20 2.2 CO_2 and air chronology

We use atmospheric CO_2 data from the WD ice core Marcott et al. (2014) which consist of 1,030 measurements between 23,000 and 9,000 years B1950 with a median resolution of 25 years. At WD, the offset in between ice and the air trapped much later at a given depth, Δage, is calculated using a firn densification model, which is constrained using nitrogen-15 data, a proxy for firn column thickness (Buizert et al., 2015). Δage ranges from 500±100 yr at the last glacial maximum, to 200±30

25 yr during the Holocene. Δage uncertainty is added to cumulative layer counting uncertainty to determine the total uncertainty of the air chronology. At EDC, Δdepth, the depth shift between synchronous air and ice levels, is calculated using an estimate of the LID based on nitrogen-15 data (Parrenin et al., 2013) that assumes negligible convective zone height.

2.3 Identifying changes in trend

We identify likely change points by taking the residuals of the linear interpolations between the change points with respect to

30 the raw data (similar to (Parrenin et al., 2013)). At the base of our method is a parallelized Metropolis-Hastings (MH) procedure
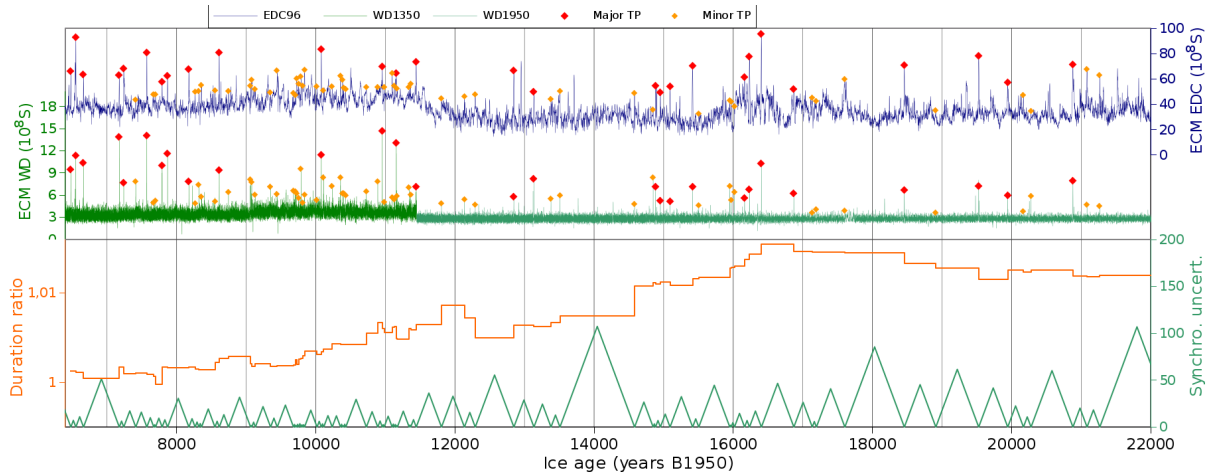
Figure 2. Volcanic synchronisation between the EDC and WD ice cores. (Top) ECM records from EDC (blue) and WD (raw data: 6.4-11.4 ka; adjusted data: 11.4-24 ka). Red diamonds show a primary set of synchronization points, selected in an initial round of visual synchronization. Orange diamonds are a secondary set of synchronization points, selected in a second round of visual synchronization. (Bottom) The ratio of the age difference between two consecutive tie points is shown in orange. The synchronization uncertainty, which is determined as 20% of the distance to the nearest tie point, is shown in green. This uncertainty is included in the calculation of leads and lags.

(Goodman and Weare, 2010; Foreman-Mackey et al., 2013). Therefore, we do not present a single "best fit" but rather analyze the ensemble of fits accepted by the routine. We plot two histograms: an upward-oriented histogram for concave-up change points, and a downward-oriented histogram for concave-down change points. We use these histograms as probabilistic locators of changes in slope (Figure 3).

5   The change point representations of the ATS2 and CO_2 time series are composed of a set of n specified change points $\{\boldsymbol{X}_i = (x_i, y_i) | i = 1, \ldots, n\}$. We denote the vector of m time series observations o at time t $\{\boldsymbol{O}_l = (t_l, o_l) | l = 1, \ldots, m\}$, and the scalar residual term J between observations and the linear interpolation between change points f_y:

$$J(\boldsymbol{X}_i) = \boldsymbol{R}^T \mathbf{C}_{obs}^{-1} \boldsymbol{R}; \ \boldsymbol{R} = \left(\frac{f_y(t_l) - o_l}{\sigma_l} \right)_l \tag{1}$$

where σ_l is the data and modeling uncertainty at l, and $\mathbf{C}_{obs}$ is the autocorrelation matrix of the residuals. Rather than inverting

10   the autocorrelation matrix, we use Cholesky and LU decompositions to solve for J, as in Parrenin et al. (2015).

We fix $x_0 = t_0$ and $x_n = t_l$; i.e. the x-values of the first and last change points are fixed to the first and last x-values of the observation vector, with the y-values allowed to vary. The remaining points are allowed to vary freely in both dimensions.

Noise can be a concern when working with time series. For our fits, the use of σ_l, the uncertainty of a data point at l, and the inverse of $\mathbf{C}_{obs}$, an estimate of the autocorrelation matrix, to weight the residuals, ensure that periodic variability and uncertain

15   data points have a minimal effect on the estimated fits. The ATS2 series contains 700 data points, and the WD CO2 series

5

contains 320, each of which is considered in the residuals. However, where data are more sparse (i.e. in the CO_2 series after the Holocene onset) change point identification becomes less precise.

2.4 Estimating the posterior probability density

In general, the probability distribution of the change points cannot be assumed unimodal, as short-timescale variations of the time series may lead to multiple modes, for example. Stochastic methods are best adapted to exploring general probability distributions (for example, Tarantola (2005)).

To tackle the large computation time required for traditional MH sampling, we apply the ensemble sampler developed by Goodman and Weare (2010) (GW) as implemented in the python emcee library (Foreman-Mackey et al., 2013). This sampler adapts the MH algorithm so that multiple model walkers can explore the probability distribution at once, making the algorithm parallelizable. It has the advantage of being affine invariant: that is, steps are adapted to the scale of the posterior distribution in a given direction.

To propose updates to the walkers, we apply what GW refer to as a "stretch move". Consider the ensemble of walkers, in this case representing potential piecewise linear fits $\mathbf{X}$ and an individual walker X_k^j in the ensemble at proposal step j. We select another walker X_h^j from the complementary ensemble $\mathbf{X}_{[k]}^j$, composed of all of the other walkers. Then, a proposal is made to update $\boldsymbol{X}_k$ to W:

$$X_k^j \rightarrow W = X_h^j + Z\left(X_k^j - X_h^j\right) \tag{2}$$

GW define the following probability distribution to generate stochastic variable Z:

$$g(Z) \propto \left\{ \frac{1}{Z} \; if \; Z \in \left[\frac{1}{a}, a\right]; \; 0 \; otherwise \right. \tag{3}$$

where a is a user-defined constant. Proposals are accepted or rejected with acceptance probability

$$P_{X_k^j \rightarrow X_k^{j+1} = W} = \min\left\{1, \; Z^{j-1}\frac{exp(-J(W)))}{exp(-J(X_k^j)))}\right\}. \tag{4}$$

We make histograms of the probable timings of 8 major change points for the WD CO_2 and ATS2 series. The choice of 8 points is not entirely arbitrary: it reflects our goal of investigating millenial-scale variability (8 points allows for approximately one point per two millenia over the study period). In addition, we can visually identify four to six major slope changes in each series (6-8 including the endpoints), though this identification is rather subjective (SI). Sensitivity tests using 7 break points (SI) produced coherent results. The results of the 8-point simulation are shown in Figure 3. The most probable timings are identified by probability peaks, or modes. We avoid comparing incoherent modes by separating changes by the sign of the second derivative of the fits. Further details of the simulations are given in the supplement.

2.5 Phasing

We estimate ρ_{lead}^{ATS2}, the probability that ATS2 leads CO_2 over a given interval, as

$$\rho_{lead}^{ATS2} = (\rho_x^{ATS2} \circ \rho_x^{CO_2}) \star \rho^{chron}, \tag{5}$$

where ρ_x^{ATS2} is the probability of a change point at time x for ATS2, $\rho_x^{CO_2}$ is the probability of a change point at time x for
5 CO_2, $\circ$ is the cross-correlation operator, which is used to calculate the probability of the difference between two variables, and
$\star$ is the convolution operator, which is used to calculate the probability of the sum of two variables. ρ^{chron} is the chronological
probability, which we take to be Gaussian centered on 0, with standard deviation $\sigma = \sigma_{chron}$ (shown in Figure 3). The intervals
associated with each change point are given in Figure 4.

3 Results and discussion

10 ## 3.1 Change point timings

The change point histograms for the ATS2 and CO_2 time series in Figure 3 confirm that the millenial-scale changes in the two
series were largely coherent. We identify five major changes in trend that occur in both series: the onset of the deglaciation from
18.1 to 17.2 ka B1950; the abrupt rise and stabilization of CO_2 and corresponding rise in temperature around 16 ka; the onset
of the Antarctic Cold Reversal (ACR) at 14.3 ka, the ACR end at around 12.7 ka, and the Holocene onset, at approximately
15 11.5 ka. For each of these changes, we calculate the probability of a lead or lag. Abrupt, centennial-scale rises in CO_2 at 16
ka, the ACR onset, and before the Holocene onset, have been identified in the WD CO_2 record Marcott et al. (2014), but their
analogs in Antarctic temperature were not previously discussed.

The deglaciation onset begins with a large, postive change point mode for Antarctic temperature, centered around 18.08 ka.
A second mode follows, at 17.70 ka. Similarly, there are two modes for the CO_2 series, centered at 17.63 ka and 17.30 ka. In
20 both series, the two modes are upward-oriented and separated by distinct antimodes. The modes appear to indicate an initial,
more gradual increase in the rate of change, followed by a sharper acceleration in both series.

CO_2 began to change even more quickly at around 16.15 ka, where we calculate a small upward-oriented probability peak.
This rise abruptly peaked at 16.07 ka, and finally stabilized at 15.9 ka. These events are both identified by downward-oriented
probability peaks. A corresponding broad, but low-probability peak in ATS2 occurs at 15.96 ka.

25 A second abrupt CO_2 rise preceded the Antarctic Cold Reversal. During this rapid rise, CO_2 experienced major sub-
centennial scale variations, and the corresponding probability peaks are noisy and large. Two narrow spikes in probability,
one at 14.64 ka, and one at 14.42 ka, mark its beginning and end. The small mode indicating the start of the CO_2 rise is not
present for the temperature series; visually, temperature appears to have accelerated more gradually. However, a sharp, unam-
biguous negative temperature change point occurs at 14.39 ka, concurrent with the CO_2 change point. Antarctic temperature
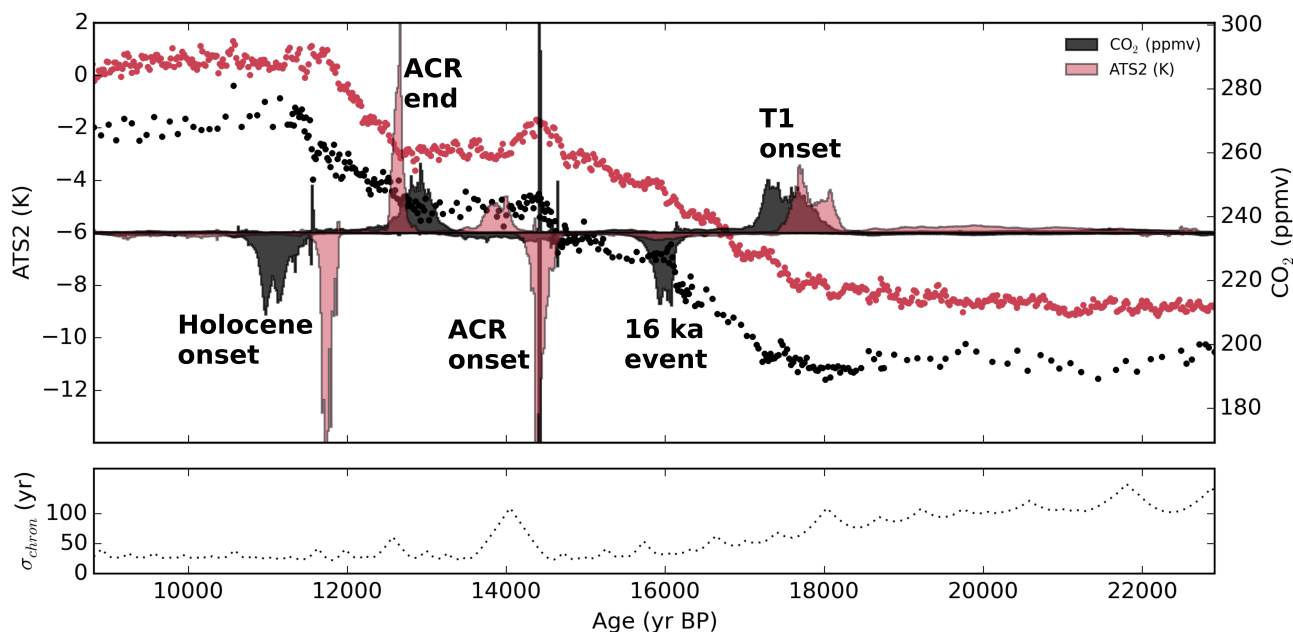
Figure 3. Upper panel: Atmospheric CO_2 (black) and ATS2 (red) placed on a common time scale, with the normalized histograms of probable change points (8 points) given below. Histograms are plotted downward-oriented when the rate of change decreases and upward-oriented when it increases (same colors, y-axis not shown, probabilities range from 0 (center) to 0.0024 (top/bottom)). In five distinct time intervals, both series show concurrent probable change points. Note the multiple modes that are often present in each of these intervals, particularly for the CO_2 series. These modes can be representative of abrupt centennial-scale change preceding a millenial-scale change, or of ambiguity in the overall trend of the series. Lower panel: Chronological uncertainty, taken as the sum of the Δage uncertainties and the uncertainty estimate for our volcanic synchronization.

began to descend rapidly after the ACR onset, finally stabilizing at the concave-up change point identified by the bimode centered on 13.98 and 13.83 ka. If a corresponding change in CO_2 occurs, it is not obvious.

The ACR terminated with an increase in CO_2, beginning at either the histogram peak around 12.9 ka or the peak at 12.8 ka. ATS2 most likely began to increase at 12.66 ka.

5   The Holocene onset is well-defined in the ATS2 series, with a large mode centered at 11.72 ka. However, multiple modes occur in the CO_2 series, which loses data resolution after the Holocene onset. A rapid rise in CO_2 occured from 11.57 to 11.53 ka. Another mode occurs at 11.31 ka. Then, two even larger modes occur in CO_2 at 11.12 and 11.01 ka. We intuit the later peaks, where data resolution is lower, to likely be indicative of higher-frequency variability or noise.
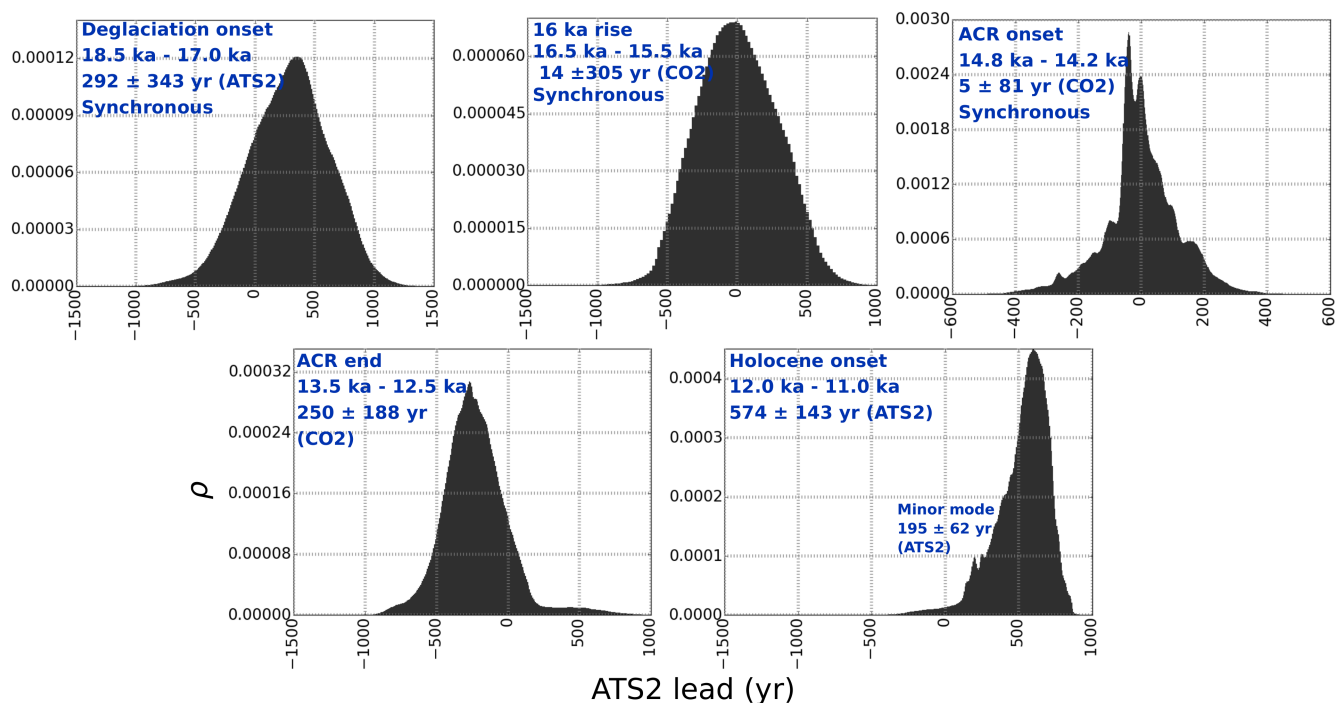
Figure 4. Probability density ρ (y-axis, normalized) of an ATS lead (x-axes, in years) at each of the selected change point intervals (noted on subfigures). Negative x-axis values indicate a CO_2 lead. In the text in each box, the name of the period, the time period in which the lead is calculated, the mean and standard deviation of the lead/lag density (μ and 1σ), and the leading variable are given.

3.2 Leads and lags

The probability that one variable leads the other over a given time period can be calculated by applying the cross-correlation operator to the histograms of the two variables over a given time period. The convolution operator can then be used to add relative dating uncertainty. The resulting probability densities are shown in Figure 4. We then report the 2 sigma standard deviation of the lead/lag, but this estimate must be applied with care where the lead probability is still multimodal, as is the case at the Holocene and ACR onsets.

ATS2 led CO_2 by 292 ± 343 years at the T1 onset. Given the large range of uncertainty, we cannot exclude the possibility of synchrony. At the peak of the 16 ka rise, CO_2 and ATS2 were synchronous, within a broad uncertainty range of 305 years, reflecting the broad probability peaks for this change. At the ACR onset, CO_2 and ATS2 were synchronous (5 ± 81 years). At the ACR end, CO_2 led ATS2, by 250 ± 188 years.

Because of the multimodality of the CO_2 change point histogram, the phasing at the Holocene onset is more ambiguous. A CO_2 lag here is certain. Calculating the phasing between 12.0 ka and 11.0 ka, we obtain an ATS2 lead of 574 ± 143 years. However, we might consider the initial stabilization in both series to be coherent, and the following CO_2 modes to be representative of sampling noise from the sudden change in data resolution. Calculating the phasing between 12.0 ka and 11.5

ka, we obtain an ATS2 lead of 195 ± 62 years. Note that this timing appears as a minor mode of the phasing calculated between 12.0 and 11.0 ka.

3.3 Discussion

Our results refine and complicate the leads and lags identified by the most recent comparable studies (Parrenin et al., 2013;
5 Pedro et al., 2012). We identify a coherent ATS2 change point not treated in these studies at 16 ka, associated with the centennial-scale rapid rise in CO_2 identified by Marcott et al. (2014).

During the major, multi-millenial scale changes which occur at T1 and Holocene onsets, Antarctic temperature likely led CO_2 by several centuries. However, during the complex, centennial-scale changes associated with the 16 ka rapid rise and the ACR onset, ATS was most likely synchronous with CO_2, and with the exception of the Holocene onset and the ACR end,
10 synchrony is within the 1σ uncertainty range of each of the phasings. At the end of the ACR, CO_2 leads temperature. And we do not identify an analog in CO_2 of the marked temperature decrease in Antarctica after the ACR onset. Additionally, many of these changes are overlayed with centennial-scale substructures identified by minor modes.

The rapid rises in CO_2 occurring at 16 ka, the ACR onset, and 11.6 ka and the Holocene onset have been identified to correspond with changes in CH_4 (Marcott et al., 2014), which are thought to originate in tropical wetland sources (Chappellaz
15 et al., 1997; Fischer et al., 2008; Petrenko et al., 2009) and are indicative of Northern Hemisphere and low-latitude temperature changes during the deglaciation (Shakun et al., 2012). Indeed, the CO_2 modes appear to demarcate the rapid changes in the WD CH_4 record, shown in Figure 5.

The beginning of a gradual rise in CH_4 at around 18 ka appears to be near-synchronous with the T1 onset rise in Antarctic temperature. This rise is not seen in Greenland paleotemperature records, where it may have been masked by AMOC-driven
20 wintertime cooling (Buizert et al., 2017) but it appears as well in proxy temperature stacks spanning both the Northern and Southern 0° to 30° latitude bands (Shakun et al., 2012).

Tephras from Mt. Takahe, a stratovolcano located in West Antarctica, have been detected in Antarctic ice cores during a 192 year interval around 17.7 ka. It has been postulated that this eruption may have provoked changes to large-scale SH circulation via ozone depletion, possibly triggering the transition between the gradual SH temperature rise beginning well before 18 ka
25 and the more rapid rise marking the deglaciation (McConnell et al., 2017). The second ATS2 mode and the first CO_2 mode we find at the deglaciation are coeval with this event within the range of dating uncertainty (Figure 5), and CH_4 visually appears to accelerate concurrently. However, the cumulative probability of the ATS2 change point is much greater before 17.7 ka than after, suggesting that additional forcings may have begun to trigger accelerated warming in the Southern Hemisphere as much as 400 years before the Mt. Takahe eruption series.
30 Paleoclimate proxies accross the globe identify abrupt changes that are coeval with the rapid rise events we identify for CO_2 and ATS2. The rapid CO_2 jumps at the ACR and Holocene Onsets may be related to Southern Ocean upwelling driven by changes in the Atlantic Meridional Overturning Circulation (AMOC) (Marcott et al., 2014), and appear in records of Asian monsoon intensity as well (Zhang et al., 2016). The 16 ka event is roughly coincident with iceberg discharge events in both
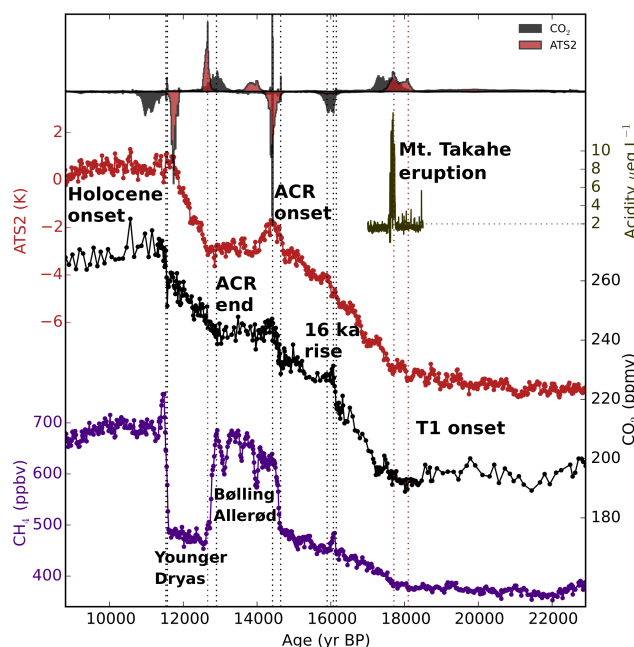
Figure 5. WD CO_2 and ATS2 change point histograms plotted with WD Acidity, ATS2, WD CO_2 and WD CH_4 series (top to bottom). Vertical lines are plotted to highlight select change point modes for the CO_2 (black) and ATS2 (red) series. CH_4 tracks changes in Northern Hemisphere climate. CO_2 modes correspond with rapid changes in CH_4 at the ACR end, ACR onset, 16 ka rise, and the rapid rise preceding the Holocene onset.

the southern and northern hemispheres (Weber et al., 2014). Here, we confirm that these events have imprints on the Antarctic temperature record.

Another notable result is the probable reversal in phasing between the T1 onset and the ACR end. These two events are structurally similar, and it has been postulated that both originate in AMOC reductions (Marcott et al., 2014). However, the

5   opposite phasings we identify indicate that if this hypothesis is valid, external conditions can modulate the timing of the effect of an AMOC change on CO_2, Antarctic temperature, or both. CH_4 appears to change nearly synchronously with CO_2 at both points, but the phasings are opposite in direction and different in magnitude. This hints at a complex coupling, depending on conditions defined by multiple other variables and mechanisms, between CO_2 and Antarctic Temperature. Centennial-scale variability may have been superimposed on coherent millenial scale trends, for example. The hypothesis that an earlier rise

10   in CO_2 at 12.9 ka, driven by land carbon loss or SH westerly winds, might have been superimposed on the millenial-scale trend (Bauska et al., 2016), is such a possible modulation. Similar complexity is evident at the ACR onset. The CO_2 rapid rise preceding the onset point is not well-marked in ATS, nor is the rapid drop in ATS well-marked in CO_2. However, the series are precisely synchronized at the peak at 14.39 ka.

The addition of the WD paleotemperature record and removal of the Vostok record from ATS2, the updated atmospheric CO_2 dataset, and our more generalized methodology are all, in part, responsible for the different time delays computed (SI). Notably, we identify change points in ATS2 that are associated with rapid rises in CO_2. We also find that several modes often exist for each change point, making the interpretation of change point timings more complex. This testifies to the importance
5 of data resolution, methodological development, and chronological accuracy in the determination of leads and lags.

4   Conclusions

Our study is a follow-up of the studies by Pedro et al. (2012) and Parrenin et al. (2013) on the leads and lags between atmospheric CO_2 and Antarctic temperature during the last deglacial warming. We refine the results of these studies by using the high resolution CO_2 record from WD; using the ice-air shift computed on WD; deriving a new Antarctic Temperature Stack
10 composed of 5 volcanically synchronized ice core isotope records; and using a more precise and complete probabilistic estimate to determine change points. Our methodology detects five major common break points in both time series. The phasing between CO2 and Antarctic climate is close but variable, with phasing ranging from a centennial-scale CO2 lead, to synchrony, to a centennial-scale lead of Antarctic climate. This variability suggests complex mechanisms of coupling. Indeed, perhaps different mechanisms of ATS2 and CO_2 rises, some coupled, others decoupled, were activated and deactivated (Bauska et al.,
15 2016) throughout the deglaciation.

Hypotheses of relationships between these events should now be reinvestigated with modeling studies. The relationship between CO_2 and Antarctic temperature on longer timescales and during other periods of rapid climate change is also of interest, as is the investigation of the role CO_2 in global temperature change. Additional high-resolution West Antarctic paleotemperature records would allow for a robust investigation of regional differences between West and East Antarctica, and our analysis
20 at the Holocene onset could be improved with continued high-resolution CO_2 measurements through the beginning of the Holocene. Our results provide modeling studies of T1 with an accurate chronological framework.

Code and data availability.

Competing interests. The authors declare that no competing interests are present for this study.

References

Barnola, J.-M., Pimienta, P., Raynaud, D., and Korotkevich, Y. S.: CO_2-climate relationship as deduced from the Vostok ice core: a re-examination based on new measurements and on a re-evaluation of the air dating, Tellus B, 43, 83–90, 1991.

Bauska, T. K., Baggenstos, D., Brook, E. J., Mix, A. C., Marcott, S. A., Petrenko, V. V., Schaefer, H., Severinghaus, J. P., and Lee, J. E.:
5   Carbon isotopes characterize rapid changes in atmospheric carbon dioxide during the last deglaciation, Proceedings of the National Academy of Sciences, 113, 3465–3470, 2016.

Berger, A.: Long-term variations of daily insolation and Quaternary climatic changes, Journal of the atmospheric sciences, 35, 2362–2367, 1978.

Buizert, C., Cuffey, K., Severinghaus, J., Baggenstos, D., Fudge, T., Steig, E., Markle, B., Winstrup, M., Rhodes, R., Brook, E., et al.: The
10   WAIS Divide deep ice core WD2014 chronology–Part 1: Methane synchronization (68–31 ka BP) and the gas age–ice age difference, Climate of the Past, 11, 153–173, 2015.

Buizert, C., Keisling, B. A., Box, J. E., He, F., Carlson, A. E., Sinclair, G., and DeConto, R. M.: Greenland-Wide Seasonal Temperatures During the Last Deglaciation, Geophysical Research Letters, pp. n/a–n/a, doi:10.1002/2017GL075601, http://dx.doi.org/10.1002/2017GL075601, 2017GL075601, 2017.

15   Caillon, N., Severinghaus, J. P., Jouzel, J., Barnola, J.-M., Kang, J., and Lipenkov, V. Y.: Timing of atmospheric CO_2 and Antarctic temperature changes across Termination III, Science, 299, 1728–1731, 2003.

Chappellaz, J., Blunier, T., Kints, S., Dällenbach, A., Barnola, J.-M., Schwander, J., Raynaud, D., and Stauffer, B.: Changes in the atmospheric CH4 gradient between Greenland and Antarctica during the Holocene, J Geophys Res Atmos, 102, 15 987–15 997, 1997.

Cuffey, K. M., Clow, G. D., Steig, E. J., Buizert, C., Fudge, T., Koutnik, M., Waddington, E. D., Alley, R. B., and Severinghaus, J. P.:
20   Deglacial temperature history of West Antarctica, Proc Natl Acad Sci U S A, 113, 14 249–14 254, 2016.

Fischer, H., Behrens, M., Bock, M., Richter, U., Schmitt, J., Loulergue, L., Chappellaz, J., Spahni, R., Blunier, T., Leuenberger, M., et al.: Changing boreal methane sources and constant biomass burning during the last termination, Nature, 452, 864, 2008.

Foreman-Mackey, D., Hogg, D. W., Lang, D., and Goodman, J.: Emcee: The MCMC Hammer, Publications of the Astronomical Society of the Pacific, 125, 306, doi:10.1086/670067, 2013.

25   Fujita, S., Parrenin, F., Severi, M., Motoyama, H., and Wolff, E.: Volcanic synchronization of Dome Fuji and Dome C Antarctic deep ice cores over the past 216 kyr, Climate of the Past, 11, 1395, 2015.

Goodman, J. and Weare, J.: Ensemble samplers with affine invariance, Comm app math comp sci, 5, 65–80, 2010.

Hays, J. D., Imbrie, J., and Shackleton, N. J.: Variations in the Earth's orbit: pacemaker of the ice ages, Science, 194, 1121–1132, 1976.

Johnsen, S., Dansgaard, W., and White, J.: The origin of Arctic precipitation under present and glacial conditions, Tellus B, 41, 452–468,
30   1989.

Jouzel, J., Masson-Delmotte, V., Cattani, O., Dreyfus, G., Falourd, S., Hoffmann, G., Minster, B., Nouet, J., Barnola, J.-M., Chappellaz, J., et al.: Orbital and millennial Antarctic climate variability over the past 800,000 years, Science, 317, 793–796, 2007.

Kawamura, K., Parrenin, F., Lisiecki, L., Uemura, R., Vimeux, F., Severinghaus, J. P., Hutterli, M. A., Nakazawa, T., Aoki, S., Jouzel, J., et al.: Northern Hemisphere forcing of climatic cycles in Antarctica over the past 360,000 years, Nature, 448, 912–916, 2007.

35   Lambert, F., Bigler, M., Steffensen, J. P., Hutterli, M., and Fischer, H.: Centennial mineral dust variability in high-resolution ice core data from Dome C, Antarctica, Climate of the Past, 8, 609–623, 2012.

Lisiecki, L. and Raymo, M.: A Plio-Pleistocene stack of 57 globally distributed benthic 0126-026180 records, Paleoceanography, 20, 2005.

Lorius, C. and Merlivat, L.: Distribution of mean surface stable isotopes values in East Antarctica; observed changes with depth in coastal area, Tech. rep., CEA Centre d'Etudes Nucleaires de Saclay, 1975.

Loulergue, L., Parrenin, F., Blunier, T., Barnola, J.-M., Spahni, R., Schilt, A., Raisbeck, G., and Chappellaz, J.: New constraints on the gas age-ice age difference along the EPICA ice cores, 0-50 kyr, Climate of the Past, 3, 527–540, 2007.

5   Lüthi, D., Le Floch, M., Bereiter, B., Blunier, T., Barnola, J.-M., Siegenthaler, U., Raynaud, D., Jouzel, J., Fischer, H., Kawamura, K., et al.: High-resolution carbon dioxide concentration record 650,000–800,000 years before present, Nature, 453, 379–382, 2008.

Marcott, S. A., Bauska, T. K., Buizert, C., Steig, E. J., Rosen, J. L., Cuffey, K. M., Fudge, T., Severinghaus, J. P., Ahn, J., Kalk, M. L., et al.: Centennial-scale changes in the global carbon cycle during the last deglaciation, Nature, 514, 616–619, 2014.

Masson-Delmotte, V., Schulz, M., Abe-Ouchi, A., Beer, J., Ganopolski, A., Gonzaález Rouco, J., Jansen, E., Lambeck, K., Luterbacher, J.,
10   Naish, T., Osborn, T., Otto-Bliesner, B., Quinn, T., Ramesh, R., Rojas, M., Shao, X., and Timmermann, A.: Information from Paleoclimate Archives, in: Climate Change 2013: The Physical Science Basis. Contribution of Working Group I to the Fifth Assessment Report of the Intergovernmental Panel on Climate Change, edited by Stocker, T., Qin, D., Plattner, G.-K., Tignor, M., Allen, S., Boschung, J., Nauels, A., Xia, Y., Bex, V., and Midgley, P., book section 5, p. 383–464, Cambridge University Press, Cambridge, United Kingdom and New York, NY, USA, doi:10.1017/CBO9781107415324.013, www.climatechange2013.org, 2013.

15   McConnell, J. R., Burke, A., Dunbar, N. W., Köhler, P., Thomas, J. L., Arienzo, M. M., Chellman, N. J., Maselli, O. J., Sigl, M., Adkins, J. F., et al.: Synchronous volcanic eruptions and abrupt climate change 17.7 ka plausibly linked by stratospheric ozone depletion, Proc Natl Acad Sci U S A, p. 201705595, 2017.

Monnin, E., Indermühle, A., Dällenbach, A., Flückiger, J., Stauffer, B., Stocker, T. F., Raynaud, D., and Barnola, J.-M.: Atmospheric CO_2 concentrations over the last glacial termination, Science, 291, 112–114, 2001.

20   NorthGRIP Project Members: High-resolution record of Northern Hemisphere climate extending into the last interglacial period, Nature, 431, 147–151, 2004.

Parrenin, F., Barker, S., Blunier, T., Chappellaz, J., Jouzel, J., Landais, A., Masson-Delmotte, V., Schwander, J., and Veres, D.: On the gas-ice depth difference (Δ depth) along the EPICA Dome C ice core, Climate of the Past, 8, 1239–1255, 2012.

Parrenin, F., Masson-Delmotte, V., Köhler, P., Raynaud, D., Paillard, D., Schwander, J., Barbante, C., Landais, A., Wegner, A., and Jouzel, J.:
25   Synchronous change of atmospheric CO_2 and Antarctic temperature during the last deglacial warming, Science, 339, 1060–1063, 2013.

Parrenin, F., Bazin, L., Capron, E., Landais, A., Lemieux-Dudon, B., and Masson-Delmotte, V.: IceChrono1: a probabilistic model to compute a common and optimal chronology for several ice cores, Geoscientific Model Development, 8, 1473–1492, 2015.

Pedro, J. B., Rasmussen, S. O., and van Ommen, T. D.: Tightened constraints on the time-lag between Antarctic temperature and CO_2 during the last deglaciation, Climate of the Past, 8, 1213–1221, 2012.

30   Pedro, J. B., Bostock, H. C., Bitz, C. M., He, F., Vandergoes, M. J., Steig, E. J., Chase, B. M., Krause, C. E., Rasmussen, S. O., Markle, B. R., et al.: The spatial extent and dynamics of the Antarctic Cold Reversal, Nature Geoscience, 9, 51, 2016.

Petit, J.-R. and Delmonte, B.: A model for large glacial–interglacial climate-induced changes in dust and sea salt concentrations in deep ice cores (central Antarctica): Palaeoclimatic implications and prospects for refining ice core chronologies, Tellus B, 61, 768–790, 2009.

Petrenko, V. V., Smith, A. M., Brook, E. J., Lowe, D., Riedel, K., Brailsford, G., Hua, Q., Schaefer, H., Reeh, N., Weiss, R. F., et al.: 14CH4
35   measurements in Greenland ice: investigating last glacial termination CH4 sources, Science, 324, 506–508, 2009.

Raynaud, D. and Siegenthaler, U.: Role of trace gases: the problem of lead and lag, Global changes in the perspective of the past, pp. 173–188, 1993.

Raynaud, D., Jouzel, J., Barnola, J., Chappellaz, J., Delmas, R., and Lorius, C.: The ice record of greenhouse gases, Science, 259, 926–926, 1993.

Shakun, J. D., Clark, P. U., He, F., Marcott, S. A., Mix, A. C., Liu, Z., Otto-Bliesner, B., Schmittner, A., and Bard, E.: Global warming preceded by increasing carbon dioxide concentrations during the last deglaciation, Nature, 484, 49–54, 2012.

5   Sigl, M., Fudge, T., Winstrup, M., Cole-Dai, J., Ferris, D., McConnell, J., Taylor, K., Welten, K., Woodruff, T., Adolphi, F., et al.: The WAIS Divide deep ice core WD2014 chronology-Part 2: Annual-layer counting (0-31 ka BP), Climate of the Past, 11, 3425–3474, 2015.

Sowers, T., Bender, M., Raynaud, D., and Korotkevich, Y. S.: δ15N of N2 in air trapped in polar ice: A tracer of gas transport in the firn and a possible constraint on ice age-gas age differences, J Geophys Res Atmos, 97, 15 683–15 697, 1992.

Tarantola, A.: Inverse problem theory, SIAM, 2005.

10 WAIS Divide Project Members and others: Onset of deglacial warming in West Antarctica driven by local orbital forcing, Nature, 500, 440–444, 2013.

Weber, M., Clark, P., Kuhn, G., Timmermann, A., Sprenk, D., Gladstone, R., Zhang, X., Lohmann, G., Menviel, L., Chikamoto, M., et al.: Millennial-scale variability in Antarctic ice-sheet discharge during the last deglaciation, Nature, 510, 134–138, 2014.

Williams, D., Peck, J., Karabanov, E., Prokopenko, A., Kravchinsky, V., King, J., and Kuzmin, M.: Lake Baikal record of continental climate response to orbital insolation during the past 5 million years, Science, 278, 1114–1117, 1997.

15 Zhang, H., Griffiths, M. L., Huang, J., Cai, Y., Wang, C., Zhang, F., Cheng, H., Ning, Y., Hu, C., and Xie, S.: Antarctic link with East Asian summer monsoon variability during the Heinrich Stadial–Bølling interstadial transition, Earth Planet. Sci. Lett., 453, 243–251, 2016.